Acknowledgment

We thank John C. Westall for providing the computer program for nonlinear least squares curve fitting to the Butler-Volmer equation.

Manuscript submitted April 14, 1986; revised manuscript received Jan. 5, 1987.

REFERENCES

1. J. R. Silkey and J. T. Yoke, *This Journal*, **127,** 1091 (1980).
2. J. S. Wilkes, J. A. Levisky, R. A. Wilson, and C. L. Hussey, *Inorg. Chem.*, **21,** 1263 (1982).
3. S. A. Bolkan and J. T. Yoke, *ibid.*, **25,** 3587 (1986).
4. S. A. Bolkan and J. T. Yoke, *J. Chem. Eng. Data*, **31,** 194 (1986).
5. Z. J. Karpinski and R. A. Osteryoung, *Inorg. Chem.*, **23,** 1491 (1984).
6. A. A. Fannin Jr., D. A. Floreani, L. A. King, J. S. Landers, B. J. Piersma, D. J. Stech, R. L. Vaughn, J. S. Wilkes, and J. L. Williams, *J. Phys. Chem.*, **88,** 2614 (1984).
7. C. L. Hussey and H. A. Øye, *This Journal*, **131,** 1621 (1984).
8. C. L. Hussey, J. R. Sanders, and H. A. Øye, *ibid.*, **132,** 2156 (1985).
9. C. J. Dymek Jr., J. L. Williams, D. J. Groeger, and J. J. Auborn, *ibid.*, **131,** 2887 (1984).
10. G. T. Cheek and R. A. Osteryoung, *Inorg. Chem.*, **21,** 3581 (1982).
11. D. D. Axtell, B. W. Good, W. W. Porterfield, and J. T. Yoke, *J. Am. Chem. Soc.*, **95,** 4555 (1973).
12. T. M. Laher and C. L. Hussey, *Inorg. Chem.*, **22,** 3247 (1983).
13. T. G. Sukhova, O. N. Temkin, and R. M. Flid, *Russ. J. Inorg. Chem.*, **15,** 949 (1970); *Zh. Neorg. Khim.*, **15,** 1849 (1970).
14. D. M. Drazic and V. Vascic, *J. Electroanal. Chem.*, **185,** 229 (1985).
15. H. Bloom, "The Chemistry of Molten Salts," pp. 94-97, W. A. Benjamin, Inc., New York (1967).
16. S. A. Bolkan, Ph.D. Dissertation, Oregon State University, Corvallis, OR (1986).
17. R. C. Howie and D. W. MacMillan, *Inorg. Nucl. Chem. Lett.*, **6,** 399 (1970).

Mass Transfer at Gas Evolving Surfaces

A Microscopic Study

Dennis W. Dees*,[1] and Charles W. Tobias**

Materials Molecular Research Division of Lawrence Berkeley Laboratory, and Department of Chemical Engineering, University of California, Berkeley, California 94720

ABSTRACT

A novel micromosaic electrode was developed to resolve the time-dependent, mass-transfer distribution in the close vicinity of bubble phenomena. The electrode, prepared on a silicon wafer using integrated circuit manufacturing technology, consists of a 10 by 10 matrix of coplanar, electrically isolated, square platinum segments on 100 μm centers, surrounded by a relatively large buffer segment. A computer actuated data acquisition and control system was assembled and the software developed to monitor the current to each of the segments and control the potential of selected segments. The effect of a single hydrogen bubble disengagement and of the coalescence of two bubbles, on the free convection limiting current of the reduction of ferric to ferrous ion was measured using the micromosaic electrode in a horizontal face-up orientation. It was found that the mass-transfer enhancement due to bubble disengagement is small when compared to that due to coalescence. Increases in the mass-transfer rate of more than an order of magnitude over the free convection limiting current were observed for the coalescence phenomena.

As with all processes occurring at gas-evolving surfaces, the mass transfer is quite complicated and not well understood. While the enhancement of the average rate of mass transfer at gas-evolving surfaces has been extensively studied, virtually nothing is known about the relative contribution of the various individual bubble phenomena. The unique properties of the micromosaic electrode (1) permit individual bubble phenomena to be controlled and their effects on the rate of mass transfer to be monitored.

Mass-transfer enhancement at gas-evolving electrodes was recognized as early as 1924 by Foerster (2). Ibl (3, 4) was one of the first investigators to attempt to quantify this effect in 1963. Since about 1970 several different electrode geometries have been studied. A great deal of work has been done on planar electrodes, oriented either horizontally (5-8) or vertically (9-12). Gas-evolving screen electrodes (13) and expanded-mesh, gas-diverting electrodes (14) have also been studied. Gas-evolution studies conducted on systems with a forced flow of electrolyte are numerous (15-18). These researches typically addressed the problem of enhancement of the mass transport by electrolytic gas evolution by macroscopic averaging of a large number of bubble phenomena on the microscale.

In the present report the mass-transport problem as it relates to the disengagement of a single bubble and the consequences of the coalescence of two bubbles followed by disengagement is addressed. Efforts to study coalescence alone were not successful because, in all cases observed, disengagement from the surface occurred simultaneously with the coalescence phenomenon.

Experimental

The micromosaic electrode.—The novel electrode, shown in Fig. 1 and conceived in our laboratory, was designed in a joint effort with Hewlett Packard Company. The micromosaic electrode was then fabricated by the Hewlett Packard Company's Technology Research Center on a 7.6 cm (3 in.) diam silicon wafer using integrated circuit technology. The actual active electrode area is the 0.5 by 0.5 cm platinum square at the center of the wafer. The lines extending radially from the electrode are aluminum current conductors that carry the current from the individual electrode segments to a set of bonding pads which are laid out in a square pattern near the edge of the wafer. The larger conductors carry the current to the buffer segment of the electrode, a relatively large section, which surrounds the center segmented area, and serves to eliminate edge effects.

A magnified view of the center portion of the wafer is shown in Fig. 2. The ten by ten matrix of square platinum segments along with 12 specially positioned segments make up the segmented portion of the micromosaic electrode. The segments in the matrix are on 100 μm centers. Each segment is 98 μm on a side, with a 2 μm gap between adjacent segments.

*Electrochemical Society Active Member.
[1]Present address: Chemical Technology Division, Argonne National Laboratory, Argonne, Illinois 60439.
**Electrochemical Society Honorary Member.

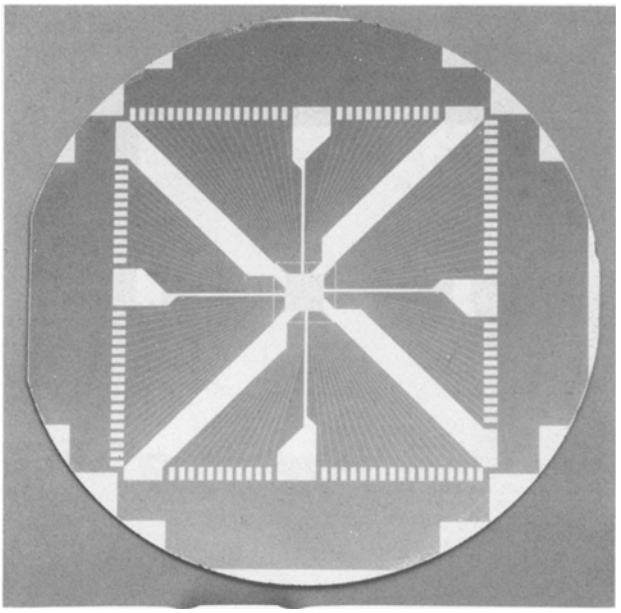

Fig. 1. Micromosaic electrode

The separate layers of material that make up the micromosaic electrode are shown in Fig. 3. Silicon oxide was grown thermally on a silicon wafer and then covered by a pore-free silicon nitride layer to form the nonconducting substrate, upon which the electrode was built. The silicon dioxide layer between the aluminum conducting layer and the platinum electrode layer extends to the inner edge of the outer square of bonding pads. It protects the aluminum layer from the electrolyte and serves to isolate each segment from the other segments. Holes were etched in the oxide to allow for electrical contact

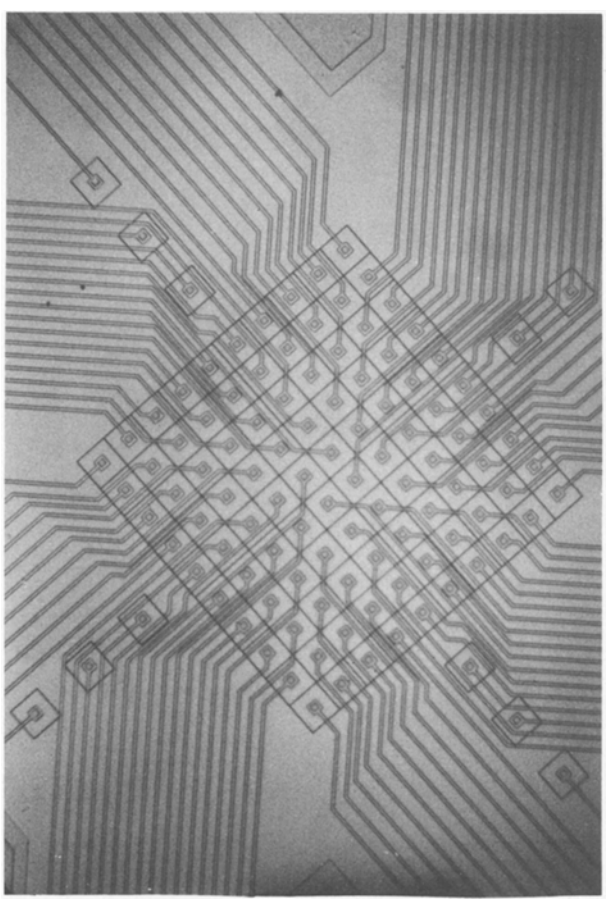

Fig. 2. Segmented portion of micromosaic electrode

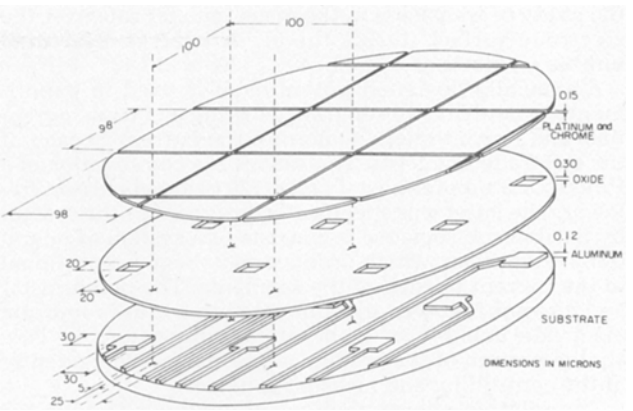

Fig. 3. Exploded view of micromosaic electrode

between the platinum and aluminum layers. A relatively thin chromium layer was placed between the platinum segments and the oxide layer to improve adherence of the platinum.

Even with the many precautions taken in the design of the micromosaic electrode, it is still quite susceptible to chemical and physical attack from the electrolyte. The attack can be so severe that it will render the electrode useless after only a few dozen experiments. A detailed description of the stability of the electrode is given in the Appendix.

The electrochemical cell.—The cell, shown in Fig. 4, is designed to accommodate the micromosaic electrode in a horizontal facing-up position. The actual cell is the cube at the center of the apparatus, which is 2.5 cm on each side. To allow observation of the micromosaic electrode surface, two counterelectrodes (total area is 2 cm^2) are placed on opposing side walls of the cell. A reference electrode capillary is built into one of the other side walls of the cell. The micromosaic electrode can be viewed through the window at the top of the cell. There are two vents in the window for gas removal, electrolyte addition, and temperature monitoring.

The cell is made of Lucite and is sealed to the micromosaic electrode with a Viton O-ring. A Lucite base serves to house and protect the electrode. Connections to the micromosaic electrode are made through the printed circuit board via a set of Zebra connectors (Series 7000 Tecknit Corporation). These connectors allow the micromosaic electrode to be replaced in a few minutes. A set of spacers attached to the base maintains proper alignment and pressure on all the components of the cell.

Instrumentation.—A data acquisition and control system was assembled and the software developed for the micromosaic electrode cell. The system was designed for

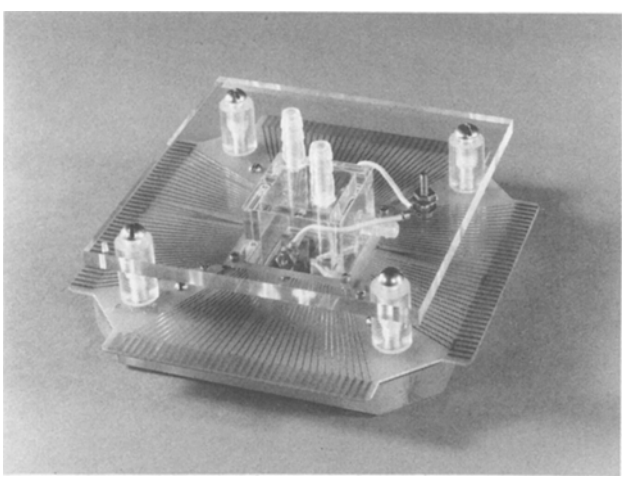

Fig. 4. Micromosaic electrode electrochemical cell with horizontal electrode orientation.

the study of transients in the mass-transfer rate over the electrode surface during the occurrence of individual bubble phenomena.

A specially designed potentiostat is used in experiments to control two separate working electrode potentials and to continuously monitor the current to each of the electrode segments. This device is a combination of a Pine RDE3 bipotentiostat and a 120 channel current follower. The latter was specifically designed for the system by Scribner Associates. It consists of a system of operational amplifiers, which produces a voltage proportional to the current to each of the segments. The potentiostat and current follower are connected to the micromosaic electrode cell by an elaborate wiring network. This analog portion of the system can be used independently of the controlling and measuring devices.

The relatively large number of channels to monitor made computer data acquisition and control a necessity rather than a luxury. A Hewlett Packard 9825T desktop microcomputer with flexible disk storage capability and a digital plotter were utilized for this task. The computer was programmed to control bubble growth and to simultaneously monitor the currents to each of the sensor segments.

Three measuring devices, which are interfaced to the computer, monitor the analog system. A 128-channel multiplexer (Neff Series 400), connected to the current follower and the potentiostat, does the bulk of the data acquisition. The multiplexer can sample at rates from 1.25 to 10.0 kHz. A Nicolet digital oscilloscope (4094) is attached to four of the current follower's channels, which in turn can be connected to any of the micromosaic electrode segments. This has proven to be quite useful for obtaining data at a faster rate than the multiplexer, and for checking the multiplexer accuracy. A Hewlett Packard 3455A digital voltmeter was used to monitor the total current going to segments where bubbles where being grown. The data from the voltmeter was used to control the growth of bubbles and to determine the time of the occurrence of the bubble phenomenon.

The computer is used to maintain a constant rate of bubble growth at one or more segments. The current to the segments where bubble growth is taking place is set by adjusting the potential of these segments. The computer is able to control the potential through a Hewlett Packard 3325A digital function generator, coupled to the potentiostat, as a digital-to-analog converter.

Both data acquisition and control aspects of the system involve real time measurements and actions by the computer. Two channels of the multiplexer are used to monitor the analog signal from a function generator that produces a triangular wave of a set amplitude and frequency. This signal is utilized by the computer to determine the precise time at which the data are taken by the multiplexer.

Method.—The classical limiting current method was employed in performing the mass-transfer experiments. The reduction of ferric ion ($Fe^{+3} + e^- \rightleftharpoons Fe^{+2}$) was used as an indicator ion reaction. Ferric sulfate was added to a well-supported aqueous electrolyte (0.05*M* $Fe_2(SO_4)$; 1.0*M* H_2SO_4). All segments were polarized negatively in the mass-transfer limiting region to reduce the ferric to ferrous ions, just positive to the potential for hydrogen evolution. The potential of specific segments were rendered 200-300 mVs more negative in order to nucleate and grow individual hydrogen bubbles. Single bubble disengagements were generated by this technique, but the coalescence of two bubbles occurred with the simultaneous disengagement of the resulting bubble. The effect of the bubble event on the mass-transfer rate was determined by monitoring the change in the limiting current to the surrounding segments at which ferric ion reduction was taking place.

Obtaining data at the specific instant of a bubble event was a particular problem. To allow resolution of mass-transfer effects, bubbles were grown slowly (15 μA/segment), and the time of their separation from the surface, or coalescence with another bubble could only be predicted within a minute. Unfortunately, with the multiplexer set at its highest sampling rate, only a few seconds of data could be stored by the computer. The problem was overcome by acquiring data continuously from the multiplexer and from the voltmeter which monitored the total current to the bubble growth segments. The bubble event is accompanied by a sudden change in the current to the bubble growth segments. This sudden change was used to trigger the computer to start saving the data about one-half second before the occurrence of the sudden change, and to set the potential of the bubble growth segments to be identical to that of the mass-transfer monitoring segments.

Results and Discussion

An abrupt change in the limiting current to the surrounding segments was measured at the time of the bubble event. The limiting current to the segments before the occurrence of the bubble phenomena was governed by free convection (1, 19), which is significantly different from the macroscopic convection found at gas evolving surfaces. Therefore the absolute size of the change in the limiting current observed for an individual bubble phenomenon is not as relevant as a comparison of the changes observed for the various phenomena.

There are a few points that one must be aware of before discussing the results of these studies. Zero time in the following graphs denotes the beginning of data acquisition, not the beginning of current passage. In all cases the micromosaic electrode had been polarized for several minutes before the beginning of data acquisition. All currents are presented as currents rather than current densities. To convert the current to a segment in microamps to a current density in milliamperes per square centimeter, one has to multiply the value by ten. Multiplying the total electrode current in milliamperes by four converts the value into milliamperes per square centimeter. It should be noted that the ordinate on the graphs of current *vs.* time has only positive values on some graphs and both positive and negative values on others. Generally, only positive values will appear on the ordinate. For these graphs a positive value indicates a cathodic current. On graphs with both positive and negative values, a cathodic current is negative and a positive value indicates an anodic current.

In the absence of any gas evolution, a small amplitude, stable, periodic variation in the free-convection limiting current to the micromosaic electrode develops after a few minutes and is shown in Fig. 5b. The current to the electrode segments also exhibits a periodic behavior, but of a much greater amplitude. A typical example is given in Fig. 5a where there is a remarkably regular periodic variation. The period of the regular fluctuations in the current to the segments is relatively constant with an average value of 29s. A comparison of the regular fluctuations in the current to segments revealed that the fluctuations are not in phase with each other. The periodic behavior of the current to segments is attributed to a cellular fluid motion near the electrode that is moving across the surface. The characteristic velocity and length of the fluid cells are 40 μm/s and 1.1 mm, respectively. The movement of the fluid cells is attributed to the secondary bulk flow in the fluid above the electrode. From the relative magnitude of the fluctuations in the current to a segment and the current to the entire electrode, it is apparent that some mechanism for averaging the electrode current is taking place. The authors have published a detailed discussion of this phenomenon (19).

The presence of a gas bubble on the electrode affects the free convection limiting current to the electrode (1). Generally the amplitude of the fluctuations decreases with the distance the segment is from the bubble generating segment. This is likely a result of the bubble hindering the free convection near its base.

A discussion of the effects of the bubble phenomena on the mass transport involves a consideration of the relative positions of the segments. The matrix numbering

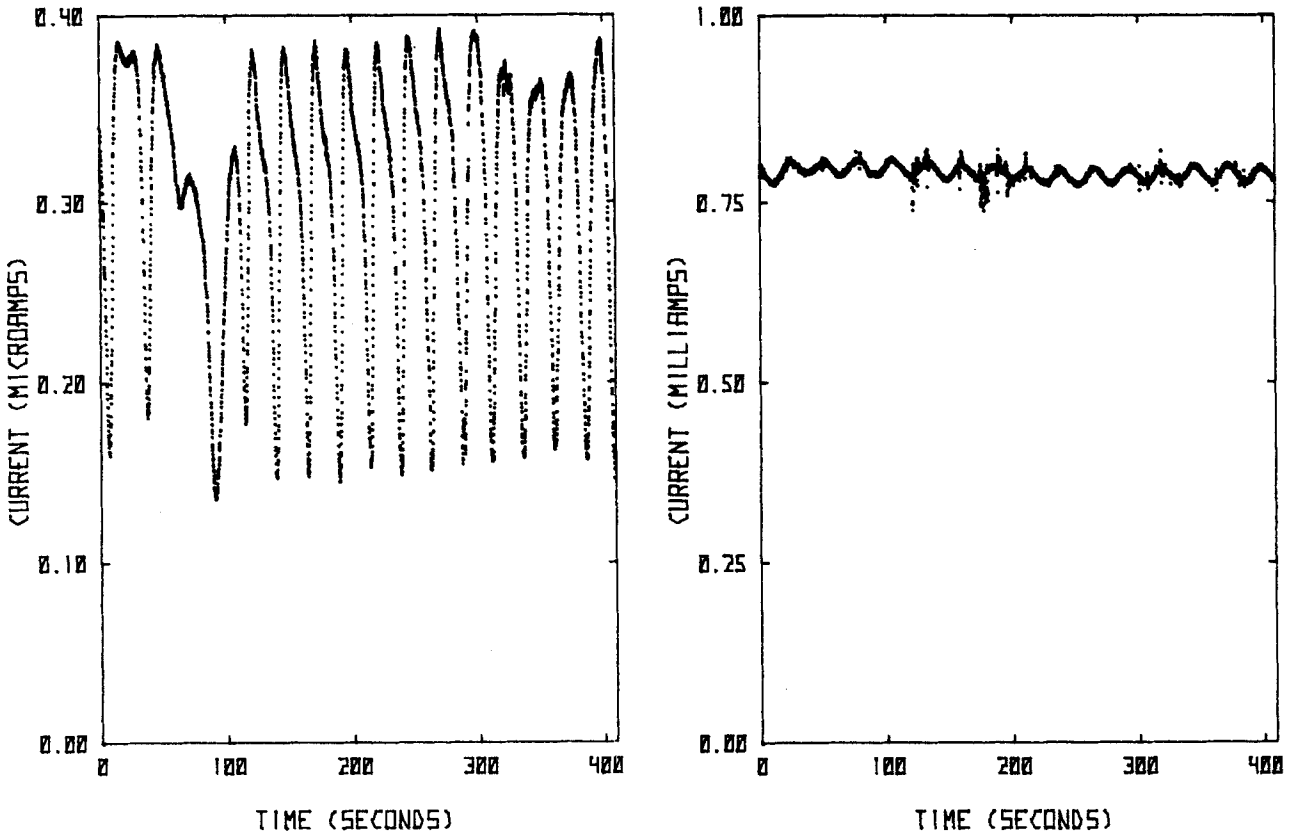

Fig. 5. Free convection limiting current; (a, left) current to a single segment; (b, right) current to the entire electrode

system adopted by the authors is given in Fig. 6. The segment in the first row and first column of the matrix of segments (*i.e.*, segment number [1,1]) is in the upper left-hand corner of the diagrams. Rows are read across the page and columns down the page.

It was found that segments having a side or corner adjacent to a segment on which a bubble was growing had a net anodic current. This anodic current can result from the oxidation of hydrogen or ferrous ions at the segment. Hydrogen generated at the bubble generating segment would be oxidized at the other segments even if the potential difference between segments was set to zero. The reaction of ferrous ions can only occur if there is a significant potential difference between segments. It should be noted that the segments adjacent to a segment with a bubble growing on it can act as bi-polar electrodes. Oxidation of ferrous ions and hydrogen can occur on one part of the segment and reduction of ferric ions on another depending on the potential distribution in the electrolyte above the segment.

It is instructive to examine the current to segments surrounding the segment at which a bubble is growing when the potential difference is set to zero. The effect on a segment with one of its sides adjacent to a bubble growth segment is given in Fig. 7a. The sudden drop in the current from 0.65 to 0.03 μA indicates that the principal reaction at the segment was the reduction of ferric ions. Since an anodic current persists after the drop, it can be concluded that hydrogen is also being oxidized at this segment. Similar behavior, shown in Fig. 7b, is exhibited by the segments with a corner adjacent to a bubble growth segment; however, in this case the current after the change is cathodic. This indicates that not as much hydrogen reaches these segments as could be expected. No such effect has been observed on any of the segments which are not immediate neighbors to a bubble growth segment.

Bubble disengagement studies.—The results of one experiment in the bubble disengagement studies demonstrated most clearly the short time effect of a bubble disengagement. The diameter of the bubble at the time of disengagement was 1.53 mm. The relative size and position of the bubble is depicted in Fig. 8.

Net anodic currents to the segments adjacent to the bubble growth segment were measured. This usually prevents the collection of any reasonable mass-transfer data from these segments; however, in this experiment the bubble did not disengage until approximately one-half second after the data acquisition was triggered. Since the potential difference is set to zero at the time that the data acquisition is triggered, the current to the segments adjacent to the bubble growth segment was cathodic for one-half second before the bubble disengagement. An example of the current to the bubble growth is given in Fig. 9a. An increase in the cathodic current at disengagement is observed.

Examining the changes in the current to segments farther away from the center of the bubble, one sees a gen-

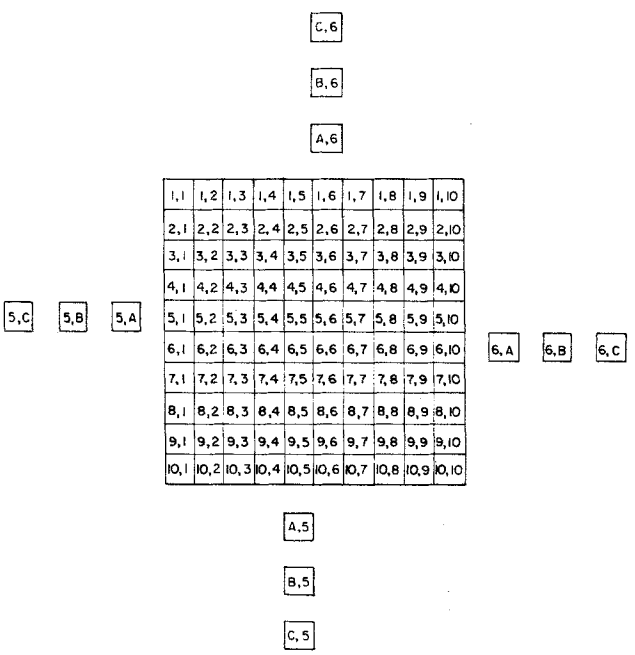

Fig. 6. Micromosaic electrode segments numbering system

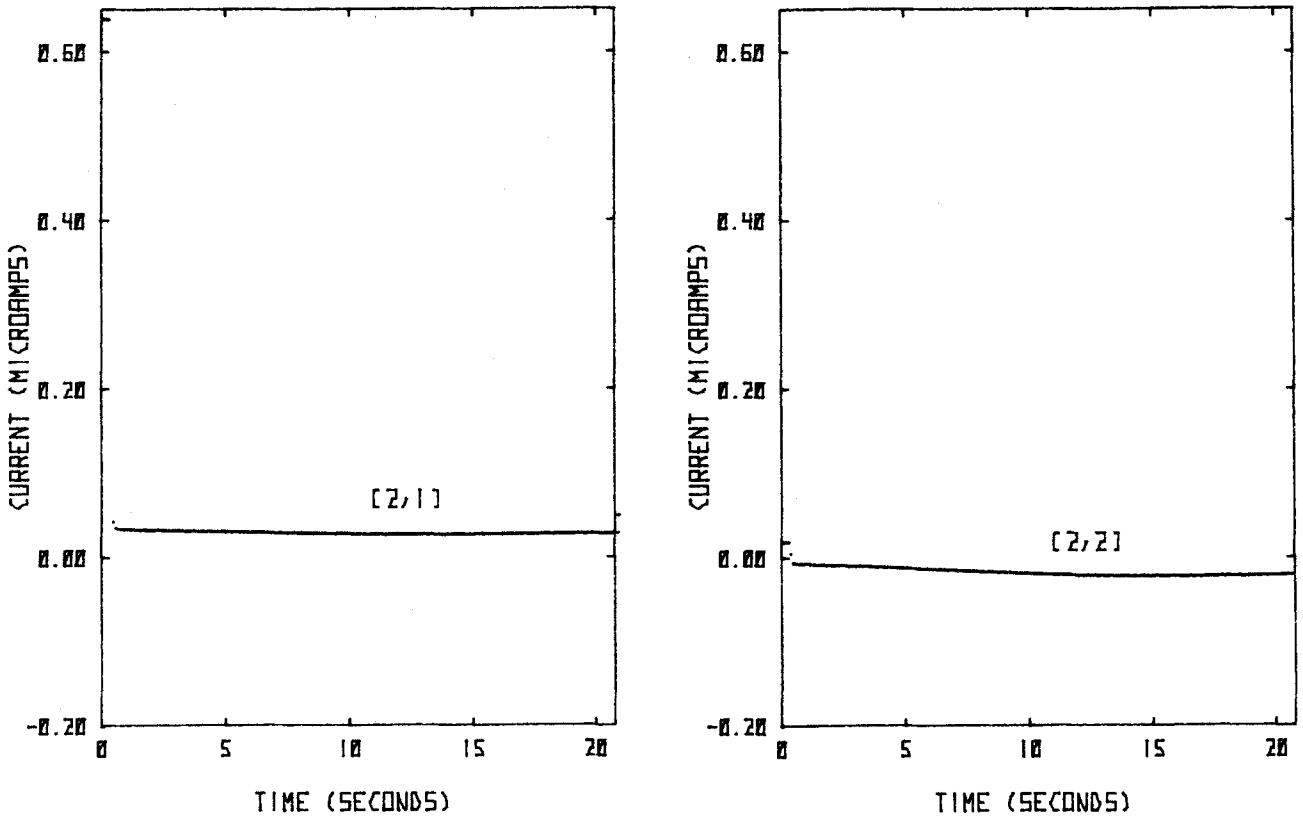

Fig. 7. Current to a segment adjacent to a bubble growth segment; potential difference is set to zero after 0.5s; (a, left) side adjacent; (b, right) corner adjacent.

eral pattern can be seen in the initial direction of the change in the current at the time of disengagement. Within 200 μm of the center of the bubble, a small absolute increase in the current is observed. At distances greater than 200 μm, but still well under the edge of the bubble, the current is seen to decrease. Near and past the perimeter of the bubble a more substantial increase in the current to segments is observed. This pattern is shown by examining Fig. 9, 10, and 11a. The segments represented in these figures form a line that extends radially outward from the center of the bubble. The same general pattern is observed in the current to segments on the opposite side of the bubble, the results of which are shown in Fig. 11b and 12. It should be noted that this behavior is generally observed independently of the magnitude of current before the event. An example of this can be seen by comparing Fig. 9b and 12a. The time constant for all the initial changes in the current is of the order of 0.1s.

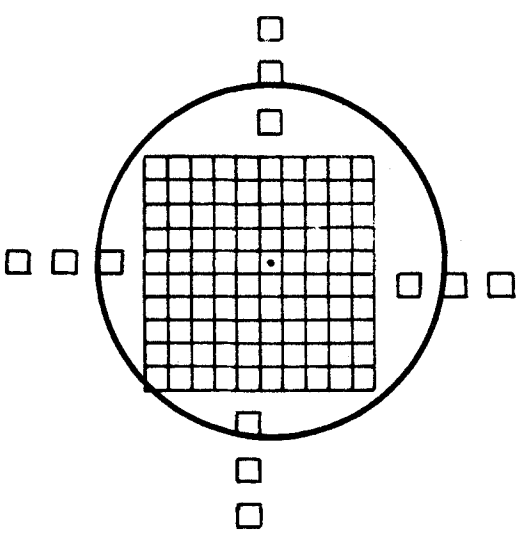

Fig. 8. Schematic of the micromosaic electrode showing the perimeter of the bubble at the time of disengagement.

While the pattern of the initial direction of the change in the current to segments surrounding the bubble is quite general, it is not universal. Generally, the deviations from the pattern for segments well under the bubble are few and do not occur over a large area. The deviations that do occur are usually found near or past the perimeter of the bubble.

It was pointed out earlier that the limiting current to the segments during bubble growth is governed by free convection. It is safe to assume that at long times after the bubble disengagement the current to segments is again governed by free convection. The abrupt change in the current to the segments surrounding the bubble at the time of its disengagement indicates that the convection generated by the bubble overcomes the free convection. This is also indicated by the general pattern of the direction of change in the current. There seems to be no consistent pattern in the change of current to the segments after the first few tenths of seconds following the beginning of the event. This can be seen by comparing the current curves from segments [2, 6] and [1, 6], in Fig. 12 to segments [8, 6] and [9, 6] in Fig. 9b and 10a. From other work (20) done in this laboratory, the time required for a single bubble of this size to disengage and rise to a height of one bubble diameter above the electrode is less than a tenth of a second. Therefore, one would not expect that the convection generated by the bubble disengagement to be important for more than a few tenths of seconds. Further, it is reasonable to believe that after this time the free convection is at least as important as the convection generated by the bubble disengagement.

It will be instructive to look at long time disengagement studies to examine free convection being reestablished after the bubble disengagement. The results from the disengagement of a 1.2 mm diam bubble will be used to illustrate this. The relative size and position of the bubble on the micromosaic electrode at the time of disengagement are depicted in Fig. 13.

The trend in the direction of change in the current to segments caused by a bubble disengagement usually

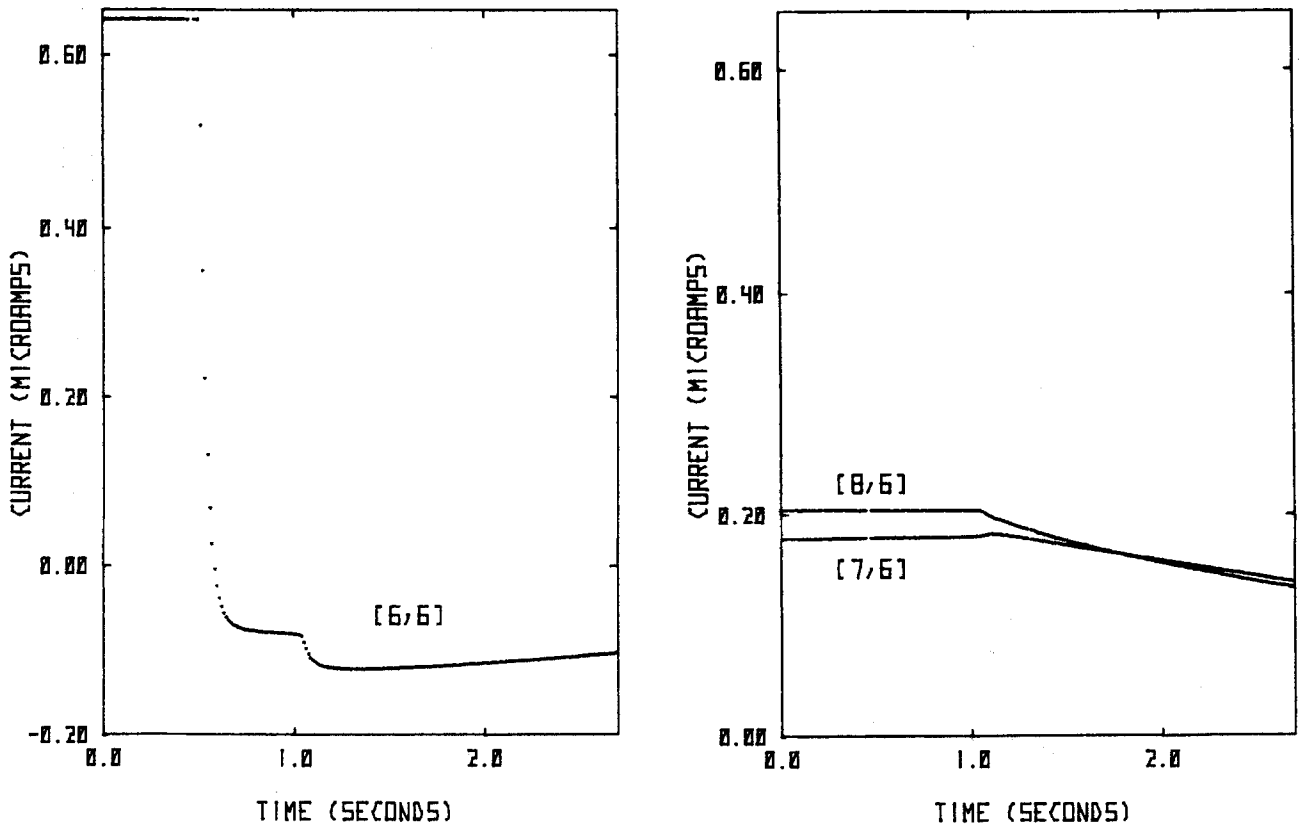

Fig. 9. Limiting current to segments before and after the disengagement of a bubble. (a, left; b, right)

persists for 1-3s. At that time the current reaches a local maximum or minimum. Following this, the current drifts relatively slowly and unpredictably for about 10-15s. An illustration of this behavior is given in Fig. 14. An initial decrease in the current is shown in Fig. 14a, and an initial increase is shown in Fig. 14b. After the 10-15s period, the free convection limiting current pattern resumes.

Taking into consideration all the observations of the current to segments before and after the bubble disengagement, the effect on the mass-transfer rate to the surface can be described. As the bubble grows the limiting current is governed by free convection. When the hydraulic and buoyancy forces exceed the surface tension forces, the bubble starts to rise and its contact area collapses. The convection generated by the disengagement

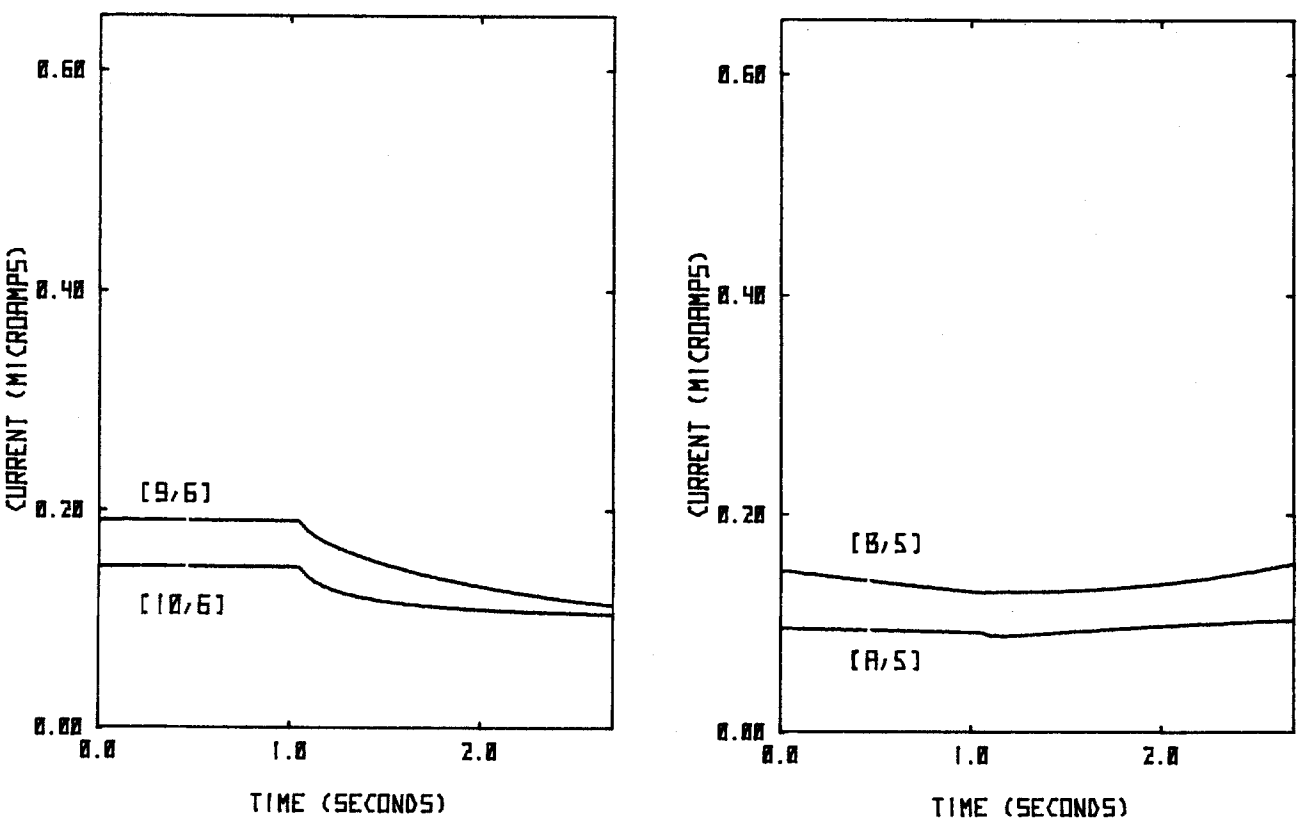

Fig. 10. Limiting current to segments before and after the disengagement of a bubble. (a, left; b, right)

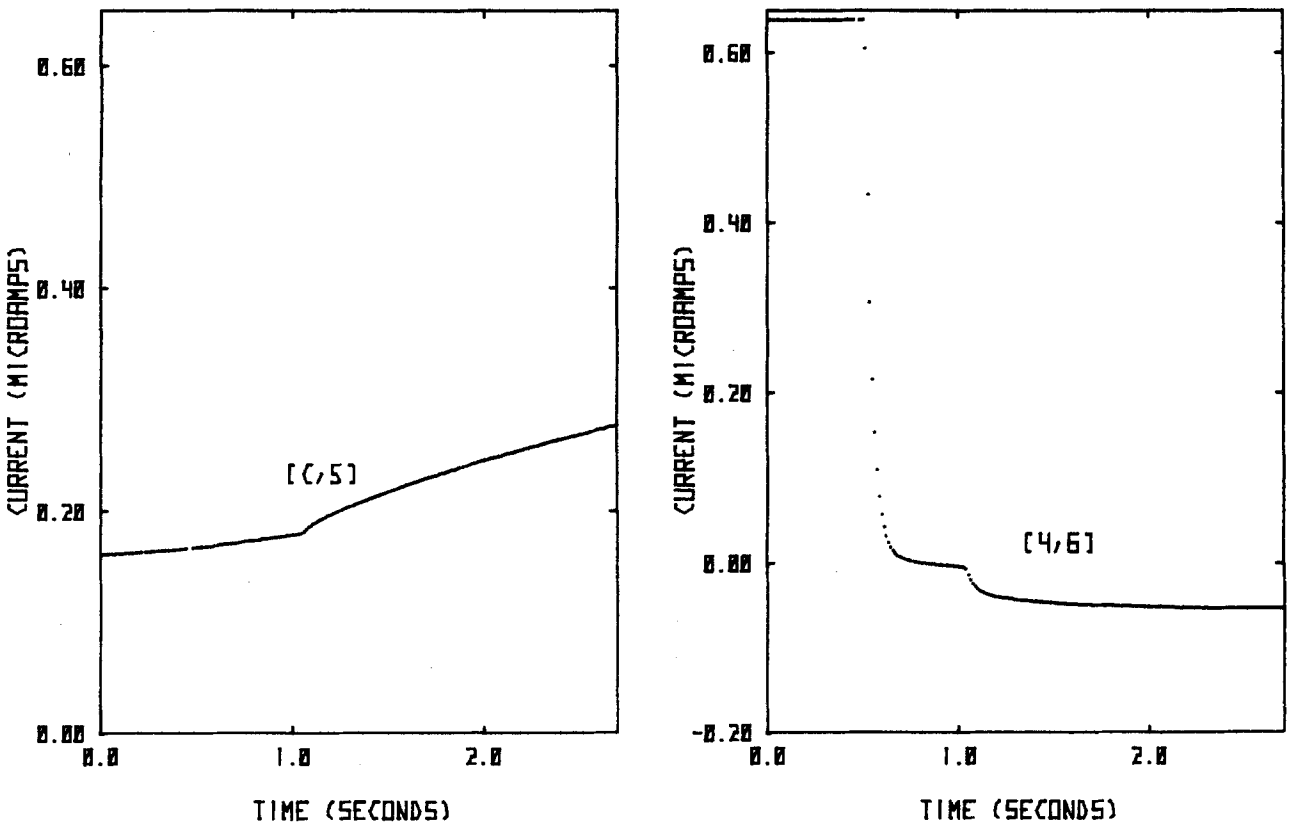

Fig. 11. Limiting current to segments before and after the disengagement of a bubble. (a, left; b, right)

and rising of the bubble causes an abrupt change in the current. After a few tenths of seconds, the bubble is several diameters away from the surface. At this point the flow generated by the bubble has little effect on the rate of mass transfer to the surface and free convection starts to dominate again. One to three seconds after the bubble disengagement free convection governs the limiting current, but another 10-15s are required to establish a steady state.

The direction of the abrupt change in the current when the bubble disengages can be explained by the flow generated by the bubble. As the bubble starts to separate from the surface the contact area collapses. Near the collapse of the contact area, the inward flow of electrolyte is

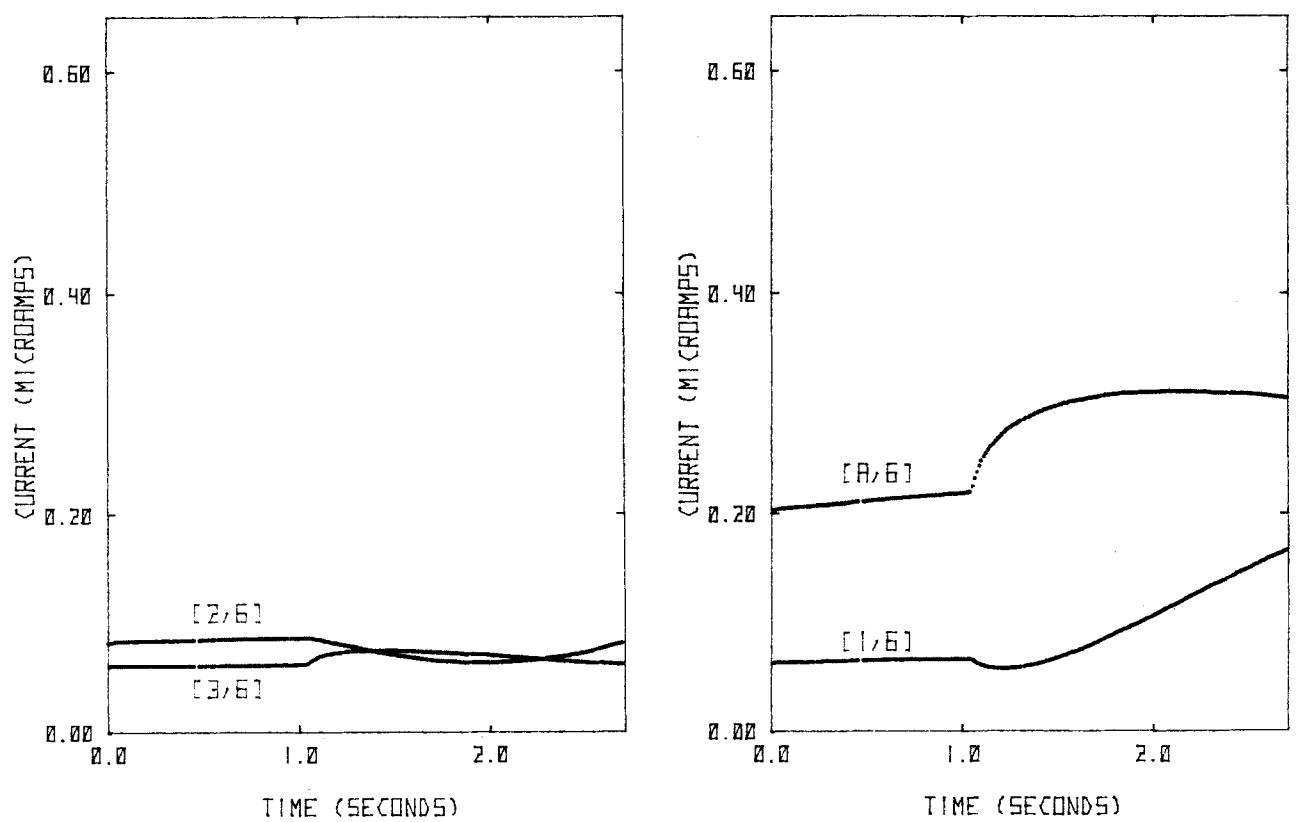

Fig. 12. Limiting current to segments before and after the disengagement of a bubble. (a, left; b, right)

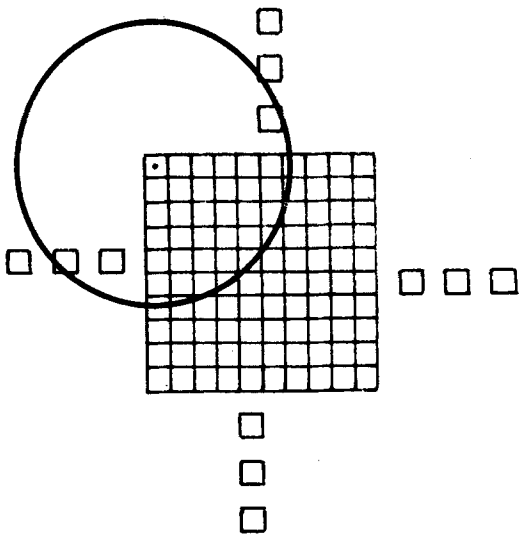

Fig. 13. Schematic of the micromosaic electrode showing the perimeter of the bubble at the time of disengagement.

turned down toward the electrode resulting in an increase in the current. When the bubble pulls loose from the electrode and rises, fluid is drawn up with the bubble and there is an inward radial flow of electrolyte. Therefore, under the bubble the direction of flow is inward and upward. Providing that the radial concentration gradients are not too great, there is a net decrease in the current as a result of the upward flow. Near and past the edge of the bubble, a recirculation flow occurs which basically involves a downward and inward movement of electrolyte causing an increase in the current.

Variations in the current from the general pattern can occur for several reasons. An asymmetric collapse of the contact area could affect the flow significantly. In addition this could induce some horizontal movement of the bubble upon release, which would also affect the flow. Both of these phenomena have been observed in this laboratory (20). An unusually large radial concentration gradient near the electrode could affect the change in the current. This would be most likely to occur near the center of the bubble and in the region around the edge of the bubble.

Simultaneous bubble coalescence and disengagement studies.—In contrast to the disengagement events, a significant increase in the rate of mass transfer was observed for simultaneous coalescence and disengagement of bubbles. Order of magnitude increases in the current to segments are not uncommon. An example of this is given in Fig. 17a where the relative size and position of the bubbles before coalescence are depicted in Fig. 15. Increases in the current were observed on nearly all the segments surrounding the bubbles, but the largest increases were observed between the bubbles along the line of coalescence.

The change in the current to the segments between two coalescing bubbles can be seen by examining the results from the coalescence and disengagement of 0.50 and 0.54 mm diam bubbles. The relative size and position of the bubbles are shown in Fig. 16. Data were obtained approximately 0.1s after the start of coalescence. The current to the segments before a bubble event occurred was often not stored by the computer. This was the result of a combination of effects: the narrow window (3s at the highest multiplexer rate) in which data could be stored by the computer and a triggering mechanism for data acquisition that was not precise enough.

The current to the segments that are located on the axis of coalescence is given in Fig. 17b and 18. Significant increases in the current are observed in all cases. The largest peak in the current exceeded the maximum value set on the multiplexer. The increase in the current is large enough and rapid enough that some distortion from the 10 Hz filters on the multiplexer inputs could have occurred tending to decrease and round off the maximum. The maximum occurs at different times for various segments, but always within less than 0.2s after zero time.

The current to segments located between the two bubbles that fall on a line perpendicular to the axis of coalescence is given in Fig. 18b and 19. Two general trends can

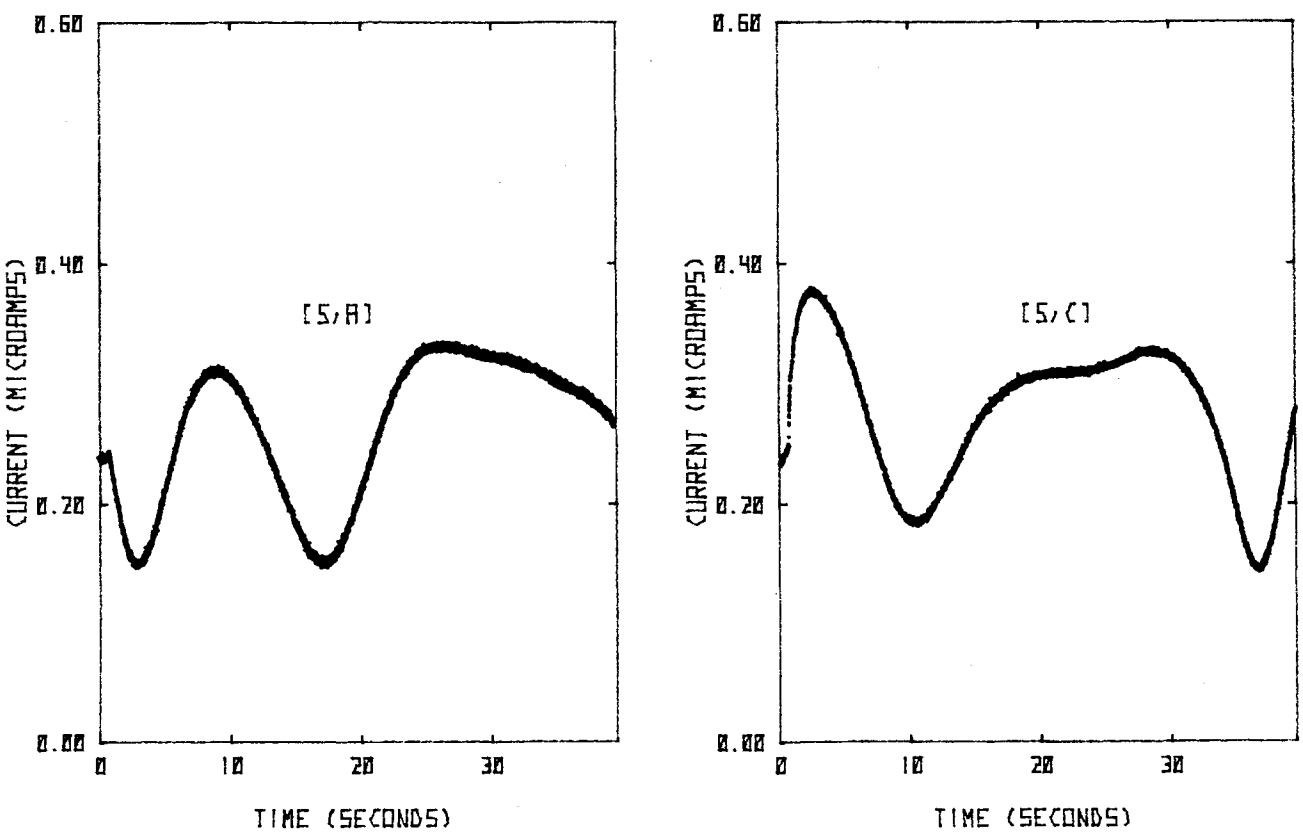

Fig. 14. Limiting current to segments before and after the disengagement of a bubble. (a, left; b, right)

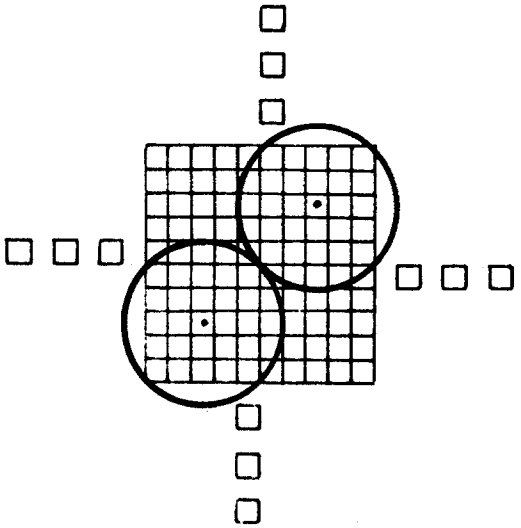

Fig. 15. Schematic of the micromosaic electrode showing the perimeter of the bubbles at the time of the event.

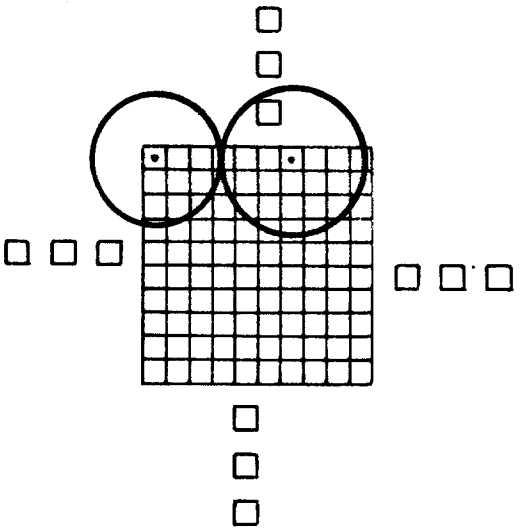

Fig. 16. Schematic of the micromosaic electrode showing the perimeter of the bubbles at the time of the event.

be observed: the height of the peak generally decreases and the peak occurs sooner the larger the distance from the line of coalescence. For these two bubbles there is very little effect 500-600 μm away from the line of coalescence.

When two bubbles coalesce, the fluid between them is squeezed out in all directions. Under and between the two bubbles there is a significant flow toward the electrode, which results in the observed peak in the current to segments located in a narrow region between the bubbles. For approximately equal size bubbles, the region is widest in the center. This would be expected from the movements of the bubbles during the occurrence of the event.

Increases in the current are also observed outside the narrow region between the bubbles. These increases are not as intense and they occur over seconds rather than within tenths of seconds. Increases in the current are observed for segments located under the bubbles. There appears to be only a small increase and sometimes a decrease in the current to segments located past the edge of the bubbles. Of the segments past the edge of the bubbles, the ones located nearest the wake created by the coalescence seem to be affected the most. This seems to be generally true of the segments located under the bubbles also. The wake formed by the bubbles during coalescence should be behind the bubbles and along the axis of the coalescence.

The long time studies of the simultaneous coalescence and disengagement reveals a behavior similar to that observed in the long time disengagement studies. After a few seconds the current is governed by free convection, but another 10-15s are required to obtain a normal stable pattern.

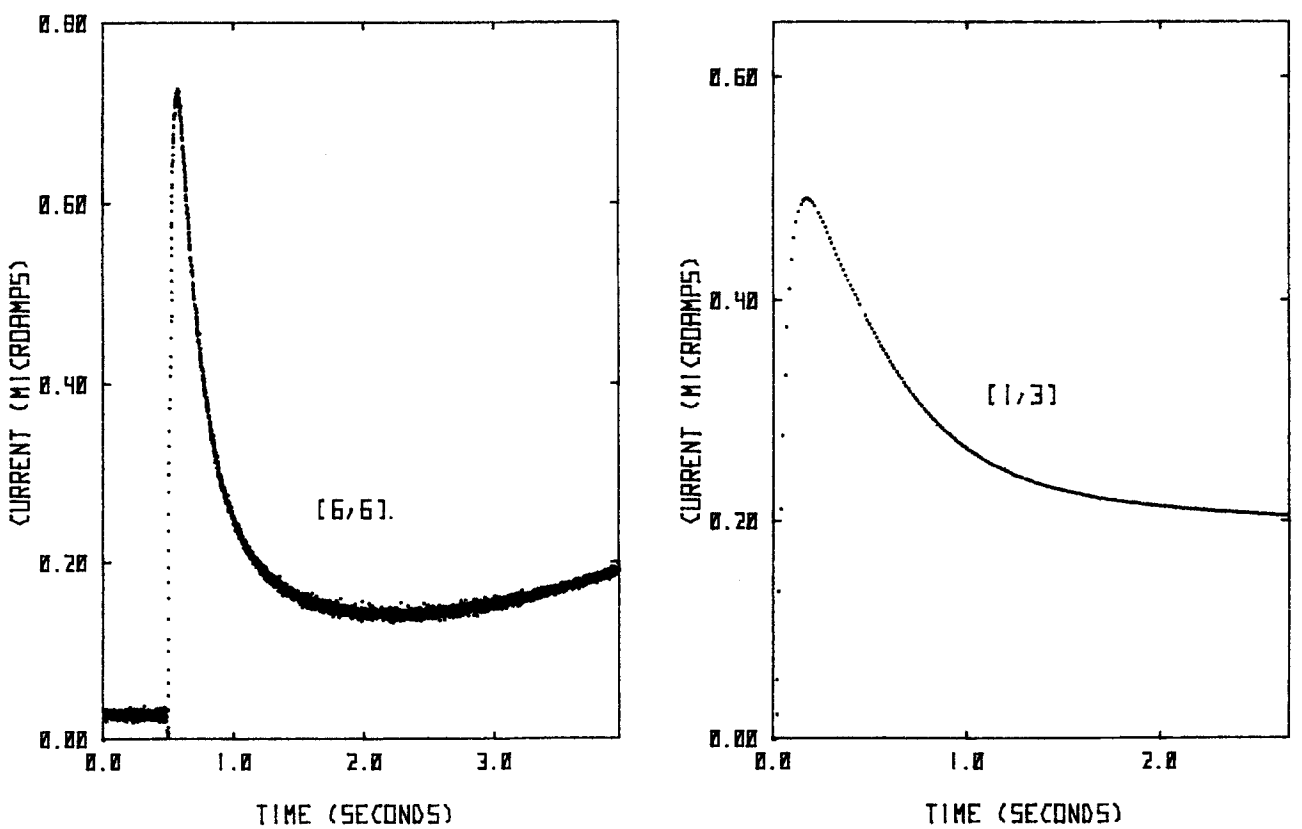

Fig. 17. Limiting current to a segment; (a, left) before and after the event; (b, right) beginning 0.1s after the event.

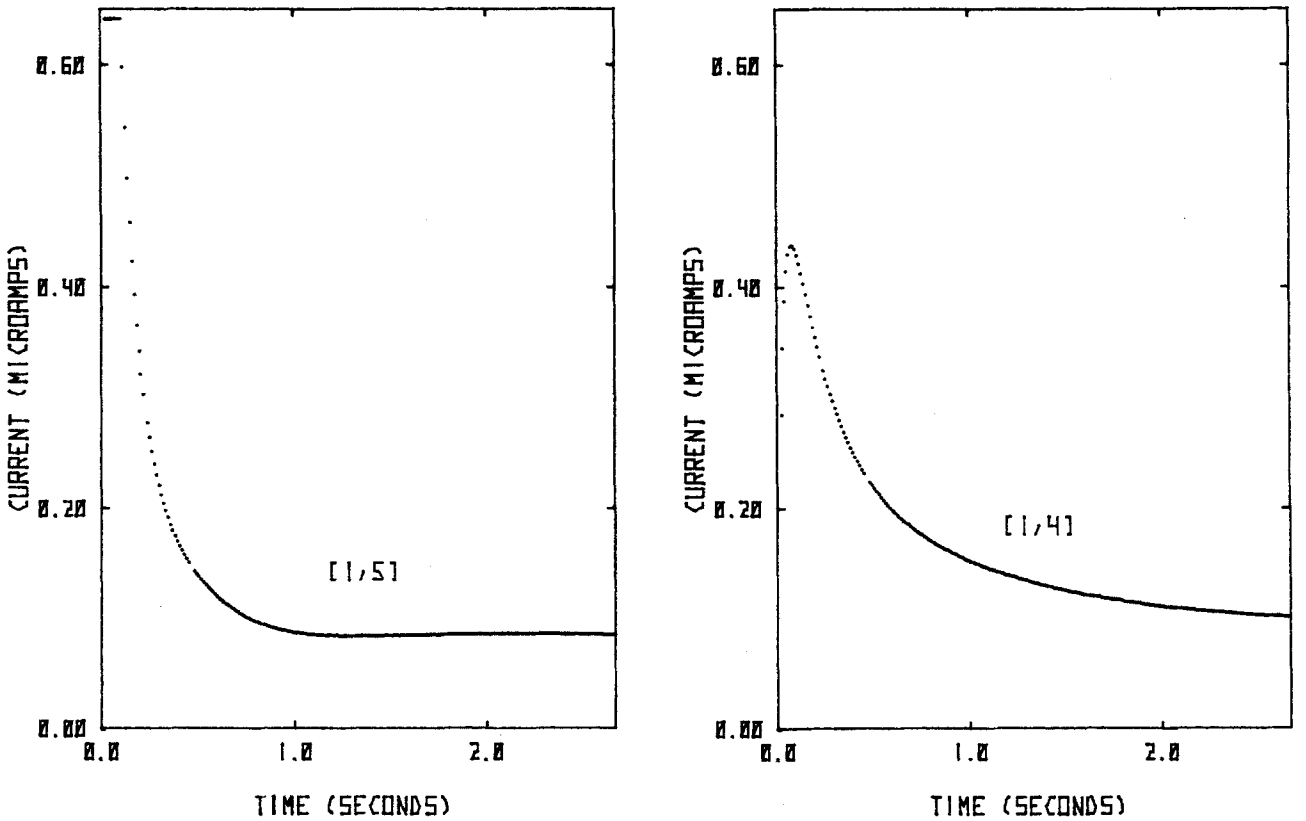

Fig. 18. Limiting current to a segment beginning 0.1s after the event. (a, left; b, right).

Conclusions

The capability of the micromosaic electrode to resolve time-dependent mass-transfer distribution in the close vicinity of bubble phenomena has been demonstrated. Results of studies on individual bubble phenomena reported in this work can be used to gain insight into the mechanism of mass-transfer enhancement at a gas-evolving surface facing horizontally upward.

The overall effect of the microconvection, generated by a bubble disengagement, on the local mass-transfer rate to a horizontal electrode is relatively small. In spite of the fact that the rate of bubble disengagements on a gas-evolving electrode can be quite high, a significant increase would not be expected. In fact, in certain adjacent regions, a net decrease in the mass-transfer rate can result from the disengagement.

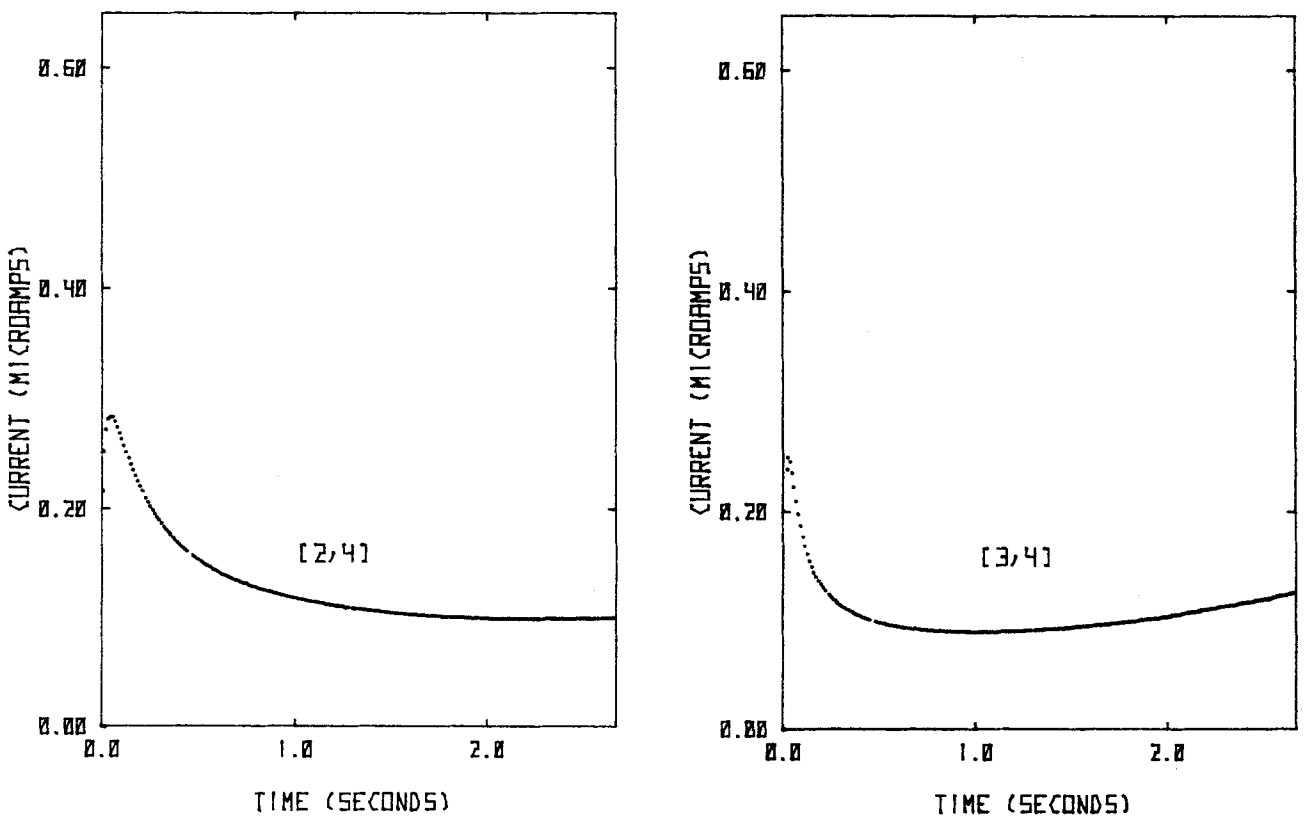

Fig. 19. Limiting current to a segment beginning 0.1s after the event. (a, left; b, right).

Significant increases have been observed in the rate of mass transfer to the surface as a result of the microconvection generated by the simultaneous coalescence and disengagement of the two bubbles. The relatively small increases observed from the disengagement studies, and the area on the electrode exhibiting the greatest enhancement effect, indicate that the high average rates of mass transfer which result from gas evolution can be attributed mainly to coalescence events. Therefore, considering the high frequency of coalescence on a gas evolving surface (8, 21, 22), coalescence induced fluid motion should provide a very effective mechanism for mass-transfer enhancement to a surface.

Acknowledgments

The authors wish to express their gratitude to the Hewlett Packard Company for making their personnel and facilities available for the fabrication of the micromosaic electrodes. This work was supported by the Assistant Secretary of Conservation and Renewable Energy, Office of Energy Systems Research, Energy Storage Division of the U. S. Department of Energy under Contract DE-AC03-76SF00098.

Manuscript submitted Sept. 2, 1986; revised manuscript received Jan. 2, 1987.

Lawrence Berkeley Laboratory assisted in meeting the publication costs of this article.

APPENDIX

Stability of the Micromosaic Electrode

Although the micromosaic electrode has proven to be a very effective experimental device for studying bubble phenomena, it is unfortunately not indestructible. The micromosaic electrode is susceptible to physical erosion and chemical corrosion when it is exposed to the experimental environment, severely limiting the useful lifetime of the electrode.

Adhesion of the platinum to the oxide is a major problem. Even the chromium layer that was added does not prevent this. A fluid flow erodes the platinum away by the drag exerted on the elements of the electrode. In addition it has been observed that a bubble upon disengaging from the electrode can cause the detachment of the segment on which it grows. This does not always occur, but after enough bubbles (*i.e.*, approximately four to six) the segment will be affected. The results of the erosion can be seen in Fig. A-1. A missing segment in the lower right-hand corner is quite visible. Gouges in the

Fig. A-2. Segments of an "old" micromosaic electrode

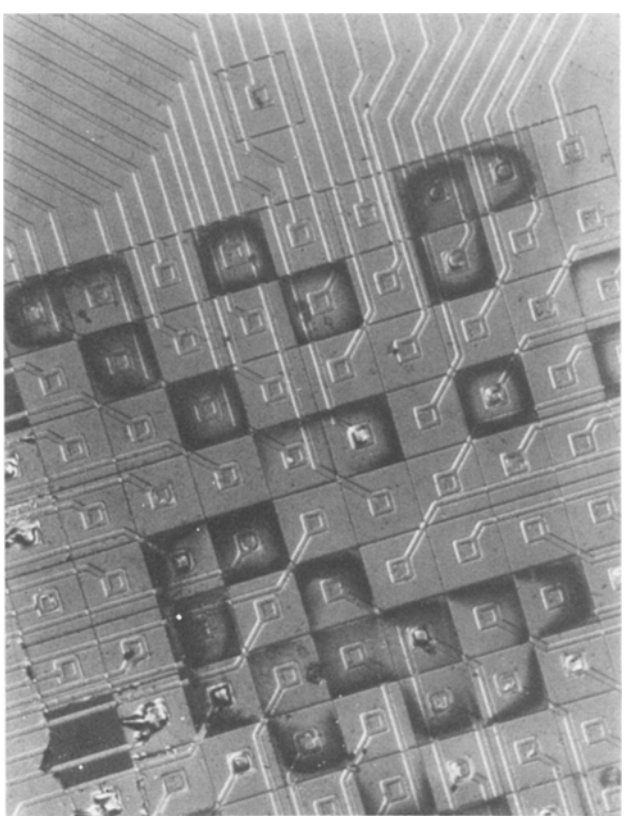

Fig. A-1. Segmented portion of "old" micromosaic electrode

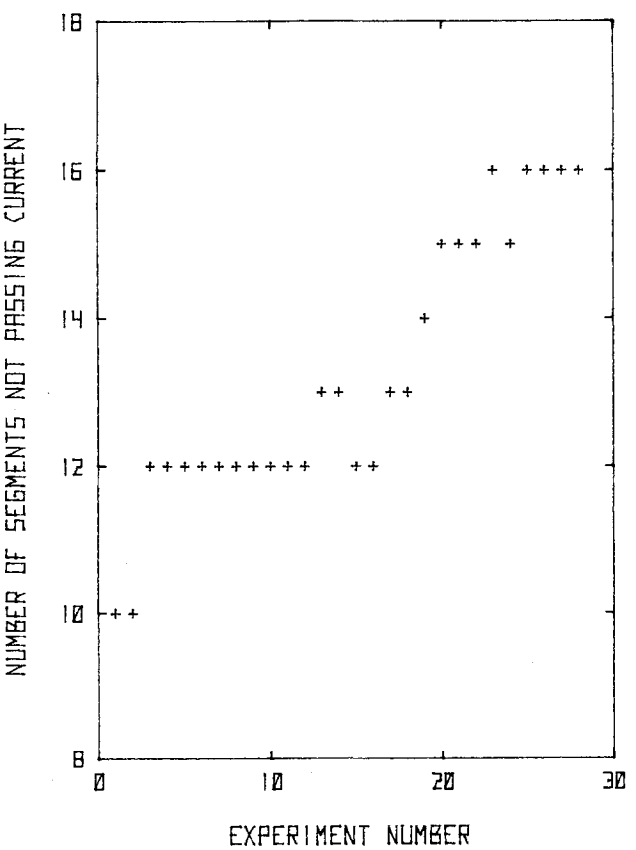

Fig. A-3. Number of defective segments during experimentation over a 24h period.

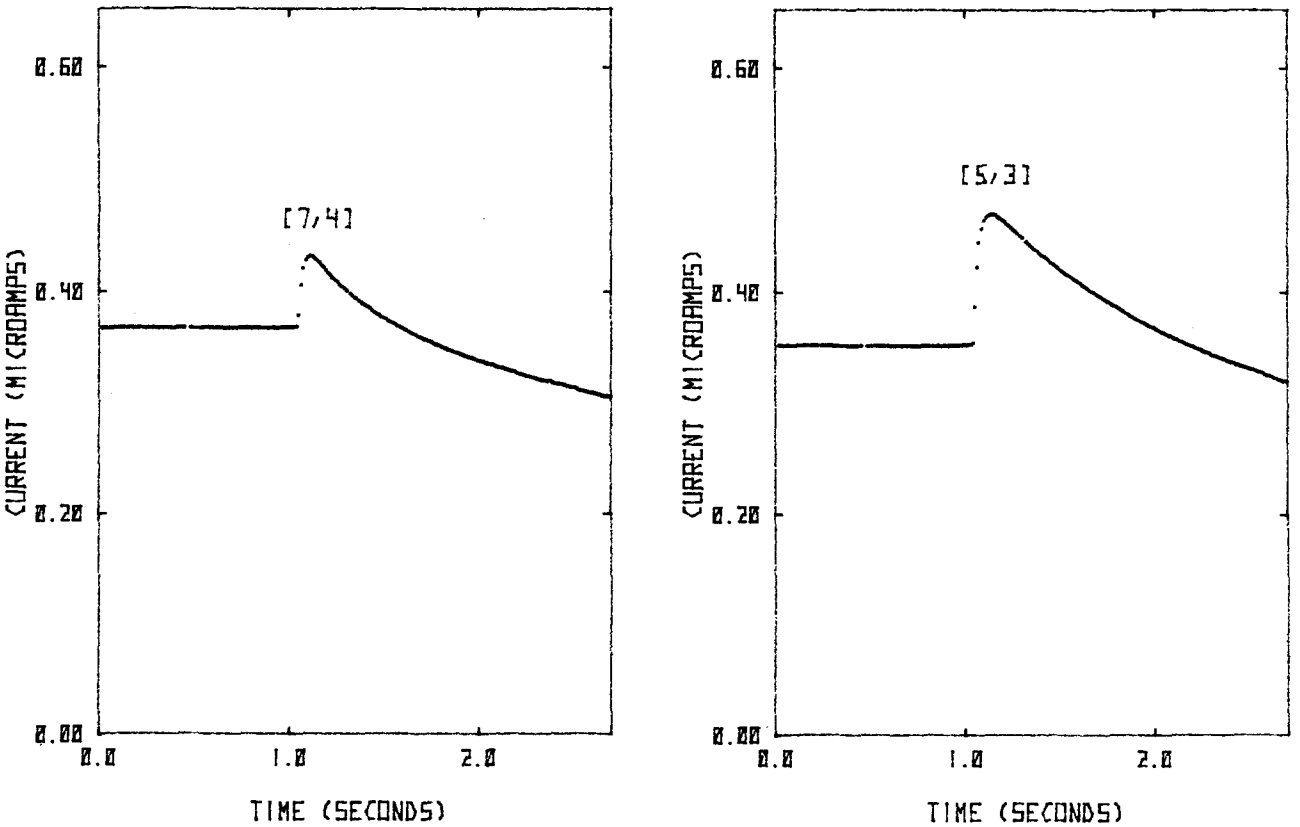

Fig. A-4. Limiting current to a segment before and after the disengagement of a bubble; (a, left) near one defective segment; (b, right) near two defective segments.

surface are also apparent. The darker segments can be seen better in Fig. A-2. The segments are darker as a result of having less platinum on the surface. Erosion is apparent from the microscopic roughness of the segments and their rounded corners.

The aluminum is subject to corrosion when it comes into contact with the electrolyte. This occurs as a result of the erosion of the platinum. Pin hole defects in the oxide layer can also expose aluminum. The rate of corrosion is relatively slow, requiring days of exposure to have a significant effect. The rate is enhanced by adding chloride ions to electrolyte, so this should be avoided.

A series of 29 experiments was conducted over a 24h period on a new electrode, at approximately equal intervals. The electrode was exposed to the electrolyte throughout the 24h. Initially ten segments on the electrode were defective. The rate at which segments stopped passing current is shown in Fig. A-3.

Of even greater importance is the fact that the electrode will degrade in the cell after it has been used. This occurs whether there is air, deionized water, or electrolyte above the electrode. The degradation is not visible or necessarily permanent, but electrode segments do stop working. The source of this degradation was not determined. Both x-ray fluorescence and scanning Auger microscopy were used to examine the atomic composition of the surface, without success. It was observed that the wetting characteristics of the oxide would change after it had been exposed to the electrolyte. Whether this is relevant to the problem was not determined.

The current to segments surrounding a defective segment was examined during bubble disengagements to determine the effect of the defective segments on the experimental results. The effect of a single bad segment is given in Fig. A-4, while the effect of two adjacent bad segments is shown in Fig. 4b. The relative size and position of the bubble on the micromosaic electrode at the time of disengagement is shown in Fig. 8. The inward fluid flow parallel to the electrode generated by the bubble disengagement can significantly enhance the mass-transfer rate when an unusually large radial concentration gradient is created by defective segments.

Once the number of defective segments reached 30-40, the assumption that the electrode simulates a continuous surface breaks down completely. Experiments that do not require this assumption can still be conducted.

REFERENCES

1. D. W. Dees, Ph.D. Thesis, Lawrence Berkeley Laboratory report LBL-16176; University of California, Berkeley (September 1983).
2. F. Foerster, *Trans. Electrochem. Soc.*, **46,** 23 (1924).
3. N. Ibl, *Chem.-Ing.-Tech.*, **35,** 353 (1963).
4. N. Ibl, E. Adam, J. Venczel, and E. Schalch, *ibid.*, **43,** 202 (1971).
5. L. J. J. Janssen and J. G. Hoogland, *Electrochim. Acta*, **18,** 543 (1973).
6. L. J. J. Janssen, *ibid.*, **23,** 81 (1978).
7. L. J. J. Janssen and E. Barendrecht, *ibid.*, **24,** 693 (1979).
8. L. J. J. Janssen and S. J. D. van Stralen, *ibid.*, **26,** 1011 (1981).
9. L. J. J. Janssen and J. G. Hoogland, *ibid.*, **15,** 1013 (1970).
10. J. Venczel, Ph.D. Thesis, University of Zurich (1961).
11. R. Alkire and P.-Y. Lu, *This Journal*, **20,** 2118 (1979).
12. M. G. Fouad, G. H. Sedahmed, and H. A. El-Abd, *Electrochim. Acta*, **18,** 693 (1973).
13. M. G. Fouad and G. H. Sedahmed, *ibid.*, **20,** 615 (1975).
14. J. Jorne and J. F. Louvar, *This Journal*, **127,** 298 (1980).
15. I. Rousar, J. Kacin, E. Lippert, F. Smirous, and V. Cezner, *Electrochim. Acta*, **20,** 295 (1975).
16. H. Hamzah and A. T. Kuhn, *J. Appl. Electrochem.*, **10,** 635 (1980).
17. I. V. Kadija and V. M. Nakic, *J. Electroanal. Chem. Interfacial Electrochem.*, **34,** 15 (1972).
18. I. V. Kadija and V. M. Nakic, *ibid.*, **35,** 177 (1972).
19. D. W. Dees and C. W. Tobias, *This Journal*, **134,** 369 (1987).
20. G. Whitney, Ph.D. Thesis, University of California, Berkeley (1987).
21. P. J. Sides and C. W. Tobias, *This Journal*, **132,** 583 (1985).
22. R. A. Putt, M.S. Thesis, University of California (1975).